

2D spatiotemporal focusing microscopy

Qiyuan Song (D2)

Abstract

We review the technique of 2-dimensional spatial temporal focusing (2D STF). STF employs ultrashort lasers pulses, which are spatially chirped by a diffractive grating, to generate the Fourier-transform-limited pulse only at a focal plane. STF offers a widefield illumination feature in two-photon excited fluorescence microscopy. 2D STF inherits this idea but uses a 2D spectral disperser to further stretch the out-of-focus pulse in spatiotemporal domain. By giving a simple mathematical analysis, we shows the improved sectioning ability of 2D STF compared with STF. 2D STF based two-photon excitation fluorescence microscopy can realize fast volume imaging. An example to trace the 3-dimensional Brownie motion is demonstrated.

Key Words: Ultrafast lasers, Laser microscopy, Fourier optics, Two-photon fluorescence microscopy

1. Introduction

Spatiotemporal focusing (STF) is a useful technique that provides widefield illumination with optical sectioning ability for multiphoton processes [1,2]. Since the sectioning ability no longer relies on a tightly focused beam spot, as in the spatial focusing scheme, it does not require a scanner to obtain a two-dimensional image. Therefore, STF offers an excellent way to decrease the illumination time. For multiphoton microscopy applications, a fast widefield imaging was realized in STF with amplified laser pulses [3,4]. For micro-fabrication applications, STF realized high-throughput 3D freeform microstructures processing [5,6]. In addition to the advantage of fast illuminating, the widefield illumination feature has been combined with photo-activated localization microscopy (PALM) or the structured light illumination (SLI) method to achieve depth-resolved super-resolution imaging [7-9]. Similarly, for optogenetic control of neuronal activity, single cell in 3D space were precisely excited by patterning the widefield illumination [10-12]. Furthermore, by combining spatial focusing with STF, the undesirable nonlinear effects were reduced in laser processing. [13].

However, since the conventional STF disperses the light only into one-dimensional (1D) space by a diffractive grating, its axial resolution is comparable to a conventional line focusing system [14]. Moreover, compared to two-photon

laser-scanning microscopy (TPLSM), the relatively high out-of-focus background limits its imaging depth [15]. For this paper, 1D STF is referred to temporal focusing with 1D spectral disperser. On the other hand, 2D STF use a 2D spectral disperser to extend 1D STF to a two-dimensional (2D) STF. The 2D spectral disperser employing a virtually imaged phased array (VIPA) generates a 2D matrix of dispersed light at a Fourier plane. The 2D spectral disperser was previously used for wavelength de-multiplexing in optical communication [16], 2D pulse shaper [17], frequency-comb spectroscopy [18] and serial time-encoded amplified imaging [19]. In 2D STF, we set the back aperture of the objective lens after this 2D matrix of dispersed light. Using this setting, at the focal plane, the pulse is Fourier-transform-limited. At the out-of-focus plane, the pulse is further stretched in the spatiotemporal domain compared to 1D STF so that the axial excitation confinement ability equals to that of a point-scanning system while we retain the widefield illumination feature.

From our analytical prediction on 2D STF, the extremely small free spectral range (FSR) is necessary for a VIPA to reduce the out-of-focus excitation by several orders of magnitude when we excite inside a sample [20]. This is a major difference from the previous work using multiline STF [21,22]. The basic advantages of 1D STF can be succeeded by 2D STF.

2. Theoretical analysis of 2D STF

In this section, we take an analytical approach for the spatiotemporal profile and axial confinement ability of 2D STF. The setup of 2D STF is shown in Fig. 1. For the 2D spectral disperser, we put the diffractive grating orthogonal to the VIPA to make the two dispersing directions of the light orthogonal to each other. Additionally, we choose the focal length of two cylindrical collimating optics to make the lateral spatial chirping length same in both directions at the Fourier plane. Inside the VIPA, the laser beam reflects multiple times back and forth and thus forms a multiple delayed beam array, which acts as a high-order grating [24]. We can describe the angular dispersion generated by VIPA after objective lens as:

$$\theta_{VIPA}(\omega) = (\gamma_{VIPA}\omega) \otimes \sum_{n=-\infty}^{+\infty} \delta(\omega - \omega_n), \quad (1)$$

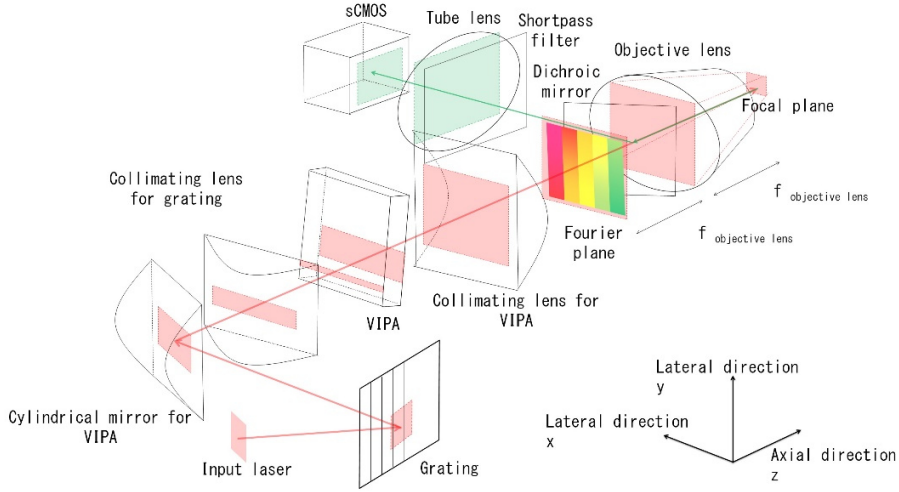


Fig. 1. Setup of 2D STF microscopy [23]

where $\theta_{VIPA}(\omega)$ is the angle of the angular dispersion at VIPA, ω is the angular frequency of the input light, and γ_{VIPA} is the constant determined by the VIPA specifications, the input angle for the VIPA [25], and the magnification ratio between the focal length of the collimating lens and objective lens. Because the free spectrum range is very small for the VIPA, different diffraction orders overlap spatially. Consequently, we take a convolution with delta functions to discriminate different diffraction orders with $\omega_{n+1} - \omega_n = 2\pi FSR$, where ω_n is the central angular frequency for the n th diffraction order and FSR is the free spectral range of the VIPA in an unit of frequency. Then at the focal plane of an objective lens, once we pre-compensate the material dispersion of the whole system, we can get Fourier-transform limited pulse as following:

$$E(x, y, \omega) = A(x, y) \left\{ E(\omega) \exp[ikx\theta_x(\omega)] \otimes \delta(\omega - \omega_c) \right\} \times \left\{ S(\omega) \exp[iky\theta_y(\omega)] \otimes \sum_{n=-\infty}^{+\infty} \delta(\omega - \omega_n) \right\}, \quad (2)$$

where $A(x, y)$ is the illumination beam profile, $E(\omega) = \exp[-(\omega/\Omega)^2]$ is the spectrum profile of the pulse with a spectrum width (FWHM) of $\sqrt{2\ln 2}\Omega$, ω_c is the central frequency. Along x direction $\theta_x(\omega) = \gamma_{Grating}\omega$ describes the linear spectrum phase generated by the grating with a constant of $\gamma_{Grating}$ which is determined by the groove density of grating and magnified by the ratio between the focal length of the collimating lens and objective lens. Along y direction $S(\omega) = \exp[-(\omega/\Omega_s)^2]$ is the diffraction

efficiency profile of each diffraction order with a spectrum width (FWHM) of $\sqrt{2\ln 2}\Omega_s$ [26, 27] and $\theta_y(\omega) = \gamma_{VIPA}\omega$ describes the linear spectrum phase in Eq. (1). To simplify calculation, we assume that the wavevector of each frequency is approximated as $k = 2\pi/\lambda_c$, the wavevector of the center wavelength of the pulse.

To obtain the spatiotemporal profile away from the focal plane, using the paraxial approximation, first we perform Fourier transform in spatial domain and add the quadratic phase due to diffraction. Then, the field becomes as following:

$$\tilde{E}(k_x, k_y, \omega, z) \propto \tilde{A}[k_x - k\theta_x(\omega), k_y - k\theta_y(\omega)] \left\{ E(\omega) \exp(-i\frac{zk_x^2}{2k}) \otimes \delta(\omega - \omega_c) \right\} \times \left\{ S(\omega) \exp(-i\frac{zk_y^2}{2k}) \otimes \sum_{n=-\infty}^{+\infty} \delta(\omega - \omega_n) \right\}, \quad (3)$$

where $\tilde{A}(k_x, k_y)$ is the Fourier transform of $A(x, y)$. In Eq. (3), we ignore all the constant phase terms that have no relationship with either the lateral position or the frequency. In order to do inverse Fourier transform back to the spatial domain, we consider the spatial change of each frequency along its own propagation direction, $k'_x = k_x - k\theta_x(\omega)$ and $k'_y = k_y - k\theta_y(\omega)$. By this view, Eq. (3) becomes as following:

$$\begin{aligned} \tilde{E}(k'_x, k'_y, \omega, z) \propto \tilde{A}[k'_x, k'_y] & \left\{ \exp \left[-i \frac{zk_x'^2}{2k} - iz\theta_x(\omega)k'_x - i \frac{zk\theta_x^2(\omega)}{2} \right] E(\omega) \otimes \delta(\omega - \omega_c) \right\} \\ & \times \left\{ \exp \left[-i \frac{zk_y'^2}{2k} - iz\theta_y(\omega)k'_y - i \frac{zk\theta_y^2(\omega)}{2} \right] S(\omega) \otimes \sum_{n=-\infty}^{+\infty} \delta(\omega - \omega_n) \right\}. \end{aligned} \quad (4)$$

In Eq. (4), we find the dispersion terms $\exp[-izk\theta_x^2(\omega)/2]$ and $\exp[-izk\theta_y^2(\omega)/2]$ which are generated from the diffraction due to the spatiotemporal coupling. By inverse Fourier transform in the spatial domain, we get

$$\begin{aligned} E(x, y, \omega, z) \propto \hat{A}(x, y) & \left\{ E(\omega) \exp \left[-i \frac{zk\theta_x^2(\omega)}{2} + ikx\theta_x(\omega) \right] \otimes \delta(\omega - \omega_c) \right\} \\ & \times \left\{ S(\omega) \exp \left[-i \frac{zk\theta_y^2(\omega)}{2} +iky\theta_y(\omega) \right] \otimes \sum_{n=-\infty}^{+\infty} \delta(\omega - \omega_n) \right\}. \end{aligned} \quad (5)$$

In Eq. (5), we can ignore the frequency dependency for $\hat{A}(x, y)$, the out-of-focus illumination beam profile. This is valid if $A(x, y)$ is much larger than the diffraction limited spot size as the case for wide field illumination. By inverse Fourier transform in temporal domain, we get

$$\begin{aligned} |e(x, y, t, z)| \propto |\hat{A}(x, y)| & \left[e'(t - k\gamma_{Grating}x) \right] \\ & \otimes \left[s'(t - k\gamma_{VIPA}y) \times \sum_{n=-\infty}^{+\infty} \delta(t - n/FSR) \right], \end{aligned} \quad (6)$$

where $e'(t) = \exp[-(t/\tau')^2]$ is the chirped pulse with half the $1/e^2$ pulse width of $\tau' = \frac{2}{\Omega} \sqrt{1 + (z/z_{Rx})^2}$,

$s'(t) = \exp[-(t/\tau'_s)^2]$ is the chirped envelope pulse with half the $1/e^2$ pulse width of $\tau'_s = \frac{2}{\Omega_s} \sqrt{1 + (z/z_{Ry})^2}$,

$z_{Rx} = \lambda_c / \pi\theta_x^2$, $z_{Ry} = \lambda_c / \pi\theta_y^2$ are the Rayleigh lengths, and

$\theta_x = \gamma_x \Omega$ and $\theta_y = \gamma_y \Omega_s$ are the dispersion angles.

Fig. 2 shows the schematics of spatiotemporal profile around focal plane. Along the propagation direction, compared with 1D STF, not only the intra pulse but also the envelope pulse are stretched. It is worthy to note that the extremely small FSR offers enough temporal displacement between each intra pulses, as shown in Fig. 2(e) and (f), which is necessary to suppress the interference effect over

hundreds of micrometer depth. Then, the two-photon excitation (TPE) intensity is further confined as following:

$$\begin{aligned} I_{TPE}(z) &= \int_{-\infty}^{\infty} \int_{-\infty}^{\infty} \int_{-\infty}^{\infty} |e(x, y, t, z)|^4 dx dy dt \\ &= I_0 / \left[\sqrt{1 + (z/z_{Rx})^2} \sqrt{1 + (z/z_{Ry})^2} \right], \end{aligned} \quad (7)$$

where I_0 is the TPE intensity at focal plane. The spatial width (FWHM) of $I_{TPE}(z)$ is $\sqrt{3}$ times as narrow as that of 1D STF whose TPE intensity distribution is proportional to $1/\sqrt{1 + (z/z_{Rx})^2}$ [14] if we set $\theta_x = \theta_y$. We can simply use the dispersion angles as the effective numerical aperture (N.A.) to evaluate the sectioning ability. Moreover, the out-of-focus TPE of 2D STF is proportional to $(1/z)^2$, which is further suppressed than that of 1D STF. Once the fluorescent material becomes optically dense, this result becomes a significant advantage for deep imaging since the intensity of the illumination light decreases along the penetration depth in an exponential function [28]. To compensate the illumination intensity decrease at the deep focal plane by increasing the laser power and at the same time to suppress the out-of-focus background generated near side of the focal plane, 2D STF will definitely outperform 1D STF.

3. 2D STF Microscopy

In this section, we will show the application of 2D STF in two-photon excitation fluorescence microscopy. In our microscopy setup, the FSR of the VIPA is 50 GHz, which corresponds to a 2-mm thickness and a refractive index of 1.5. The groove number of the grating is 150 lines/mm, the input angle for the VIPA in air is set as 0.05 rad and the input beam width is 90 μm . The focal length of the collimating optics for the grating and the VIPA are 1000 mm and 400 mm. The objective lens is UPLSAPO 60XW (Olympus) with N.A. of 1.2. With this design, the dispersion angles, θ_x and θ_y are around 0.75 and the back aperture of the objective lens will cut the tail of the spectrum matrix. In order to get enough peak power, we use a chirped pulse amplification (CPA) laser source with a central wavelength of 803 nm, a

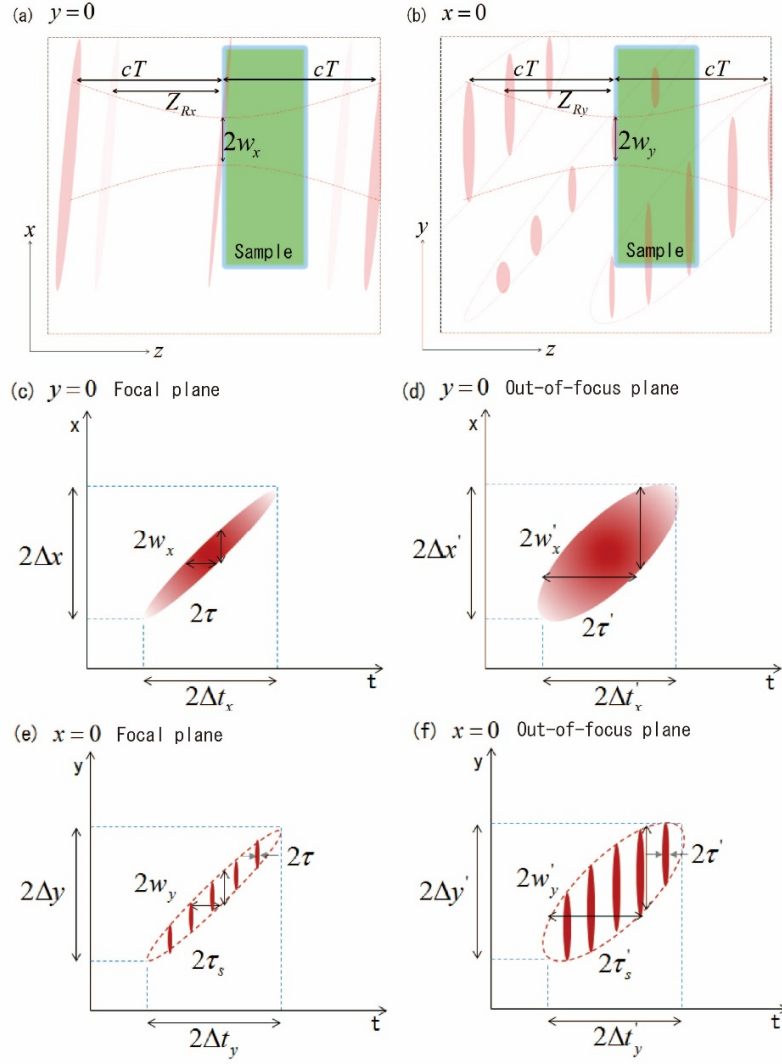


Fig. 2 Spatiotemporal profile of 2D STF: the cross section of pulse around focal plane at $y=0$ (a) and $x=0$ (b), the light speed is c , the period of pulse is T , the transient $1/e^2$ beam width along x and y direction are $2w_x$ and $2w_y$; (c) the spatiotemporal profile of single period along x direction in (a) at focal plane and (d) out-of-focus plane, the $1/e^2$ Fourier transform limited pulse width is 2τ , the $1/e^2$ illumination beam width is $2\Delta x$ at focal plane and $2\Delta x'$ out-of-focus plane, the scanning time is $2\Delta t_x$ at focal plane and $2\Delta t'_x$ out-of-focus plane; (e) the spatiotemporal profile of single period along y direction in (b) at focal plane and (f) out-of-focus plane, the $1/e^2$ Fourier transform limited envelope pulse width is $2\tau_s$, the $1/e^2$ illumination beam width is $2\Delta y$ at focal plane and $2\Delta y'$ out-of-focus plane, the scanning time is $2\Delta t_y$ at focal plane and $2\Delta t'_y$ out-of-focus plane.

pulse duration of ~ 50 fs (FWHM), and a repetition rate of 1 kHz. We also integrate a piezo stage and a scientific CMOS (sCMOS) camera for the imaging system in order to achieve fast scanning in z direction and 2D single shot imaging. Limited by the acquisition time of sCMOS camera, the imaging region is limited to 128 by 216 pixels for every single shot imaging with a frame rate of 1 kHz. By scanning

in z direction, we capture a volume image of $17.8 \mu\text{m}$ by $10.6 \mu\text{m}$ by $5.4 \mu\text{m}$ (z) at 50 volumes per second.

As a demonstration, we trace the Brownian motion of a $1 \mu\text{m}$ fluorescent bead [29]. When there are lots of beads close to each other, a displacement less than the radius of bead is necessary to discriminate the target bead from

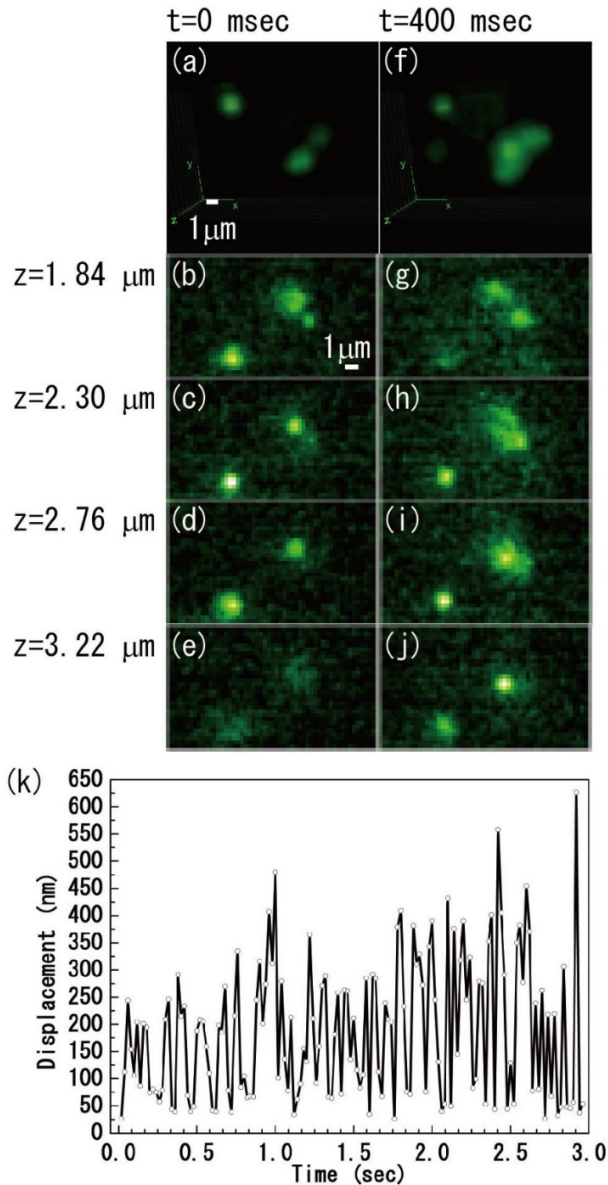


Fig. 3 Brownie motion: (a) volume imaging of $1\mu\text{m}$ beads at 0 msec, (b)-(e) lateral slices of volume imaging of (a) at selected axial positions, (f) volume imaging of $1\mu\text{m}$ beads at 400 msec, (g)-(j) lateral slices of (f) at selected axial positions, (k) measured 3D displacement of left upper bead in (a) over 3 sec.

neighbor beads during movement. Otherwise, we will confuse with many possible trajectories. In order to realize this, the root mean square (RMS) displacement of movement between neighbor frames should be less than the radius of the bead. Since the RMS displacement is proportional to $\sqrt{\Delta t}$ where $1/\Delta t$ is the volume rate, our system which has a volume rate of 50 Hz can offer a RMS displacement around

240 nm according to the calculation [30]. It is roughly half of the radius of the bead and is able to trace the random path of Brownian motion. Fig. 3 (k) shows the measured displacements during a few seconds. We use weighted algorithm to determine centroid with sub-pixel resolution. The measured RMS displacement is 226 nm, which matches well with the numerical calculation.

4. Conclusion

A 2D STF system is able to increase the confinement ability, both axial resolution and out-of-focus TPE, and simultaneously maintain the fast widefield illumination property of 1D STF. We theoretically analyzed the spatiotemporal profile of 2D STF and confirmed the axial confinement ability. We also demonstrated 50 Hz volume imaging to trace 3-dimensional Brownie Motion with 2D STF microscopy.

Reference

1. D. Oron, E. Tal, and Y. Silberberg; *Opt. Express* **13** (2005) 1468.
2. G. H. Zhu, J. van Howe, M. Durst, W. Zipfel, and C. Xu: *Opt. Express* **13** (2005) 2153.
3. L. C. Cheng, C. Y. Chang, C. Y. Lin, K. C. Cho, W. C. Yen, N. S. Chang, C. Xu, C. Y. Dong, and S. J. Chen: *Opt. Express* **20** (2012) 8939.
4. O. D. Therrien, B. Aubé, S. Pagès, P. D. Koninck, and D. Côté: *Biomed. Opt. Express* **2** (2011) 696.
5. D. Kim and P. T. C. So: *Opt. Lett.* **35** (2010) 1602.
6. Y. C. Li, L. C. Cheng, C. Y. Chang, C. H. Lien, P. J. Campagnola, and S. J. Chen: *Opt. Express* **20** (2012) 19030.
7. A. Vaziri, J. Y. Tang, H. Shroff, and C. V. Shank: *Proc. Natl. Acad. Sci. U.S.A.* **105** (2008) 20221.
8. H. Choi, E. Y. S. Yew, B. Hallacoglu, S. Fantini, C. J. R. Sheppard, and P. T. C. So: *Biomed. Opt. Express* **4** (2013) 995.
9. K. Isobe, T. Takeda, K. Mochizuki, Q. Song, A. Suda, F. Kannari, H. Kawano, A. Kumagai, A. Miyawaki, and K. Midorikawa: *Biomed. Opt. Express* **4** (2013) 2396.
10. E. Papagiakoumou, F. Anselmi, A. Bègue, V. D. Sars, J. Glückstad, E. Y. Isacoff, and V. Emiliani: *Nat. Methods* **7** (2010) 848.
11. E. Papagiakoumou, A. Begue, B. Leshem, O. Schwartz, B. M. Stell, J. Bradley, D. Oron, and V. Emiliani: *Nat. Photonics* **7** (2013) 274.
12. A. Bègue, E. Papagiakoumou, B. Leshem, R. Conti, L. Enke, D. Oron and V. Emiliani: *Biomed. Opt. Express* **4** (2013) 2869.
13. R. Kammel, R. Ackermann, J. Thomas, J. Gotte, S. Skupin, A. Tunnermann and S. Nolte: *Light Sci. Appl.* **3** (2014) e169.
14. M. E. Durst, G. Zhu, and C. Xu: *Opt. Commun.* **281** (2008) 1796.
15. M. E. Durst, A. A. Straub, and C. Xu: *Opt. Lett.* **34** (2009) 1786.
16. S. Xiao and A. M. Weiner: *Opt. Express* **12** (2004) 2895.
17. V.R. Supradeepa, C. B. Huang, D. E. Leaird and A. M. Weiner: *Opt. Express* **16** (2008) 11878.
18. S. A. Diddams, L. Hollberg, and V. Mbele: *Nature* **445** (2007) 627.
19. K. Goda, K. K. Tsia and B. Jalali: *Nature* **458** (2009) 1145.
20. Qiyuan Song, A. Nakamura, K. Hirotsawa, K. Isobe, K. Midorikawa, and F. Kannari: *Rev. Sci. Instrum.* (submitted).
21. E. Papagiakoumou, V. de Sars, V. Emiliani, and D. Oron: *Opt. Express* **17** (2009) 5391.
22. A. Vaziri and C. V. Shank: *Opt. Express* **18** (2010) 19654.
23. Q. Song, A. Nakamura, A. Isouchi, K. Hirotsawa, K. Isobe, K. Midorikawa and F. Kannari: *Biomedical Optics, Technical Digest*

(online), (Optical Society of America, Miami, 2014), paper BT3A.25.

24. M. Shirasaki: *Opt. Lett.* **21** (1996) 366.
25. A. Vega, A. M. Weiner, and C. Lin: *Appl. Opt.* **42** (2003) 4152.
26. S. Xiao, A. M. Weiner, and C. Lin: *IEEE J. Quant. Electron.* **40** (2004) 420.
27. G. H. Lee and A. M. Weiner: *J. Lightwave Technol.* **23** (2005) 3916.
28. A. K. Dunn, V. P. Wallace, M. Coleno, M. W. Berns, and B. J. Tromberg: *Appl. Opt.* **39** (2000) 1194.
29. Q. Song, K. Isobe, K. Hirosawa, K. Midorikawa, F. Kannari : *Photonics West: BIOS, Technical Digest* (online), (SPIE, San Francisco, 2015), paper 9329-92. (in press)
30. R. M. Mazo, *Brownian Motion: Fluctuations, Dynamics, and Applications* (Oxford University Press, 2009).